DOI 10.1007/s10812-019-00803-7
*Journal of Applied Spectroscopy, Vol. 86, No. 2, May, 2019 (Russian Original Vol. 86, No. 2, March–April, 2019)*

# CROSS SECTIONS, TRANSITION INTENSITIES, AND LASER GENERATION AT THE $^3P_1 \rightarrow {}^3H_5$ TRANSITION OF $LiY_{0.3}Lu_{0.7}F_4:Pr^{3+}$ CRYSTAL

**A. S. Nizamutdinov,[a] O. S. Morozov,[a] S. L. Korableva,[a] V. V. Semashko,[a] E. B. Dunina,[b] A. A. Kornienko,[b] M. P. Demesh,[c*] N. V. Gusakova,[c] A. S. Yasukevich,[c] V. E. Kisel,[c] and N. V. Kuleshov[c]**

UDC 535.34;535.37

*Lasing and spectroscopic properties of an $LiY_{0.3}Lu_{0.7}F_4:Pr^{3+}$ crystal grown by the Bridgman–Stockbarger method were investigated in detail. Absorption and luminescence spectra were recorded using polarized light. Lifetimes of excited states $^3P_J$ were determined. Absorption and emission transition intensities were calculated according to f–f-transition intensity theory taking into account interconfiguration interaction. Stimulated emission transverse cross sections were determined using the Füchtbauer–Ladenburg method. Pumping by an InGaN laser diode produced continuous-wave laser generation at 522.6 nm ($^3P_1 \rightarrow {}^3H_5$) in Pr-doped mixed fluoride crystals with a maximum output power of 0.38 W and a slope efficiency of 19%.*

***Keywords:*** *praseodymium, mixed fluorides, absorption, luminescence, visible laser.*

**Introduction.** Solid-state visible lasers have recently stimulated continuous interest because of significant technical progress in InGaN (GaN) laser diodes (LDs) emitting in the blue–violet spectral range that includes absorption bands of ions used for visible generation ($Pr^{3+}$, $Tb^{3+}$, $Sm^{3+}$, $Eu^{3+}$, etc.) [1]. At present, $Pr^{3+}$ in fluoride crystals seems most promising because efficient visible generation is obtained in these materials [2–4]. Figure 1 shows an energy level diagram of $Pr^{3+}$.

Mixed fluoride crystals of the $LiY_xLu_{1-x}F_4$ type with the scheelite structure have interesting distributions of activator ions in the matrix depending on the ratio of $Y^{3+}$ and $Lu^{3+}$ cations. The distribution coefficient of $Ce^{3+}$ increased from three to five times in mixed $LiY_xLu_{1-x}F_4$ crystals for $x$ = 0.6–0.8 [5]; for $Nd^{3+}$, practically doubled for $LiY_{0.35}Lu_{0.65}F_4$ crystal [6, 7] as compared with $LiYF_4$ (YLF) and $LiLuF_4$ (LLF) crystals. Analogous behavior was expected for $Pr^{3+}$ because ionic radii in the series $Ce^{3+}$–$Nd^{3+}$ are similar [5–7]. Previously, generation was obtained in the $^3P_0 \rightarrow {}^3H_6$ transition (~640 nm) in $LiY_{0.3}Lu_{0.7}F_4:Pr^{3+}$ crystal [8].

The present work investigated the laser spectroscopic properties of an $LiY_{0.3}Lu_{0.7}F_4:Pr^{3+}$ crystal. Generation in the $^3P_1 \rightarrow {}^3H_5$ transition with $\lambda_{em}$ = 522.6 nm was observed for the first time. This transition was chosen because of the special significance of its second harmonic for biological applications.

**Experimental.** $LiY_{0.3}Lu_{0.7}F_4:Pr^{3+}$ crystals were grown by the Bridgman–Stockbarger method in a graphite crucible with an excess of high-purity Ar gas pressure using a seed crystal for oriented crystallization. Starting components (>99.995% pure) were crystallized beforehand and used in nonstoichiometric ratios with a small excess of LiF because of incongruent melting of $LiY_{0.3}Lu_{0.7}F_4$ crystals, which was characteristic of YLF homologs [9]. The amount of $PrF_3$ in the melt ($C_0$) was determined from the $YF_3$–$LuF_3$ ratio and reached 1 (sample 1) and 2 at.% (sample 2). The first crystal was used for laser experiments; the second, for spectroscopic studies. The density of the grown crystals was 5.6 g/cm$^3$.

Absorption and luminescence spectra were recorded using polarized light with the electric field vector **E** directed parallel (π) and perpendicular (σ) to the crystal optical axis on a Cary 5000 spectrophotometer with spectral slit width 0.09 and 0.30 nm for ranges 425–620 and 970–2600 nm. Steady-state visible luminescence was measured with 0.07-nm resolution using a system with an MDR-23 monochromator, Hamamatsu C5460 module, and Stanford SR830 lock-in amplifier.

*To whom correspondence should be addressed.

[a]Institute of Physics, Kazan Federal University, Kazan, Russia; [b]Vitebsk State Technological University, Vitebsk, Belarus; [c]Center for Optical Materials and Technologies, Belarusian National Technical University, 22 Ya. Kolas Str., Minsk, 220013, Belarus; email: maxim.demesh@bntu.by. Translated from Zhurnal Prikladnoi Spektroskopii, Vol. 86, No. 2, pp. 203–209, March–April, 2019. Original article submitted December 20, 2018.

 

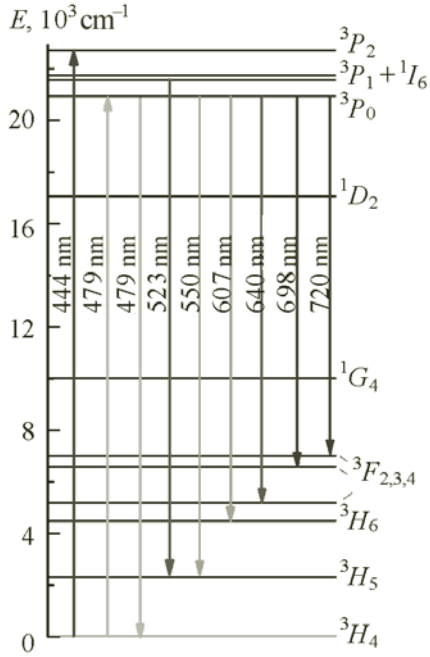


Fig. 1. Energy level diagram of $Pr^{3+}$.

Luminescence was excited by a GaN-LD with λ = 444 nm. The spectral sensitivity of the luminescence system was calibrated using a halogen lamp to produce the true shape of the spectrum [10].

Decay of excited states $^3P_J$ of $Pr^{3+}$ was studied using exciting radiation from an LT-2214 optical parametric generator (LOTIS TII) with $\lambda_{em}$ = 444 nm and pulse length ~20 ns. Luminescence radiation passing through an MDR-12 monochromator was recorded at ~640 nm by a Hamamatsu C5460-01 module and a digital oscilloscope with a bandwidth of 500 MHz.

The Judd–Ofelt approach is widely used to calculate intensities in spectra of lanthanide ions but gives unsatisfactory results for $Pr^{3+}$ because low-lying excited *f–d*-configurations affect the intensities of intraconfiguration *f–f*-transitions. Therefore, *f–f*-transition intensity theory with moderate interconfiguration interaction (ICI) was used [12] and took into account the final energy of the transition initial and final multiplets $E_J$ and $E_{J'}$ and energy $E_f^0$ of excited configuration $4f^{N-1}5d$. The transition electric-dipole (ED) line strength was

$$S_{\mathrm{ED}}\left(JJ'\right) = \sum_{k=2,4,6} \Omega_k \left[1 + 2R_k\left(E_J + E_{J'} - 2E_f^0\right)\right] \left\langle 4f^n\left[SL\right]J \left\| U^{(k)} \right\| 4f^n\left[S'L'\right]J' \right\rangle \ , \tag{1}$$

where $\Omega_k$ are intensity parameters; $R_k$, parameters due to configuration interaction. Values of doubled matrix elements $\|U^{(k)}\|$ were approximated as an intermediate bond for the free ion. The contribution of a magnetic-dipole (MD) mechanism to the overall transition probability was taken into account by determining the absorption and emission oscillator strengths. Line strength *S* was converted to oscillator strength *f* using a well-known formula from the literature [11]. Oscillator strengths of absorption transitions were determined from the obtained absorption spectra using the formula

$$f_{\mathrm{exp}}\left(JJ'\right) = \frac{mc^2}{\pi e^2 N_{\mathrm{Pr}} \overline{\lambda}^2} \int \frac{\alpha_{JJ'}^{\pi}\left(\lambda\right) + 2\alpha_{JJ'}^{\sigma}}{3} \, d\lambda \ , \tag{2}$$

where $\overline{\lambda}$ is the weighted mean transition wavelength; $\alpha_{JJ'}^{\pi,\sigma}$, integrated absorption coefficient for the corresponding polarization state. The sought variables $\Omega_k$ and $R_k$ were determined by a least-squares method by fitting theoretical oscillator strengths to the experimental ones. The radiative lifetime of the $^3P_0$ level was calculated using the obtained $\Omega_k$ and $R_k$ values and the transition probability formula [11].

**Results and Discussion.** The $Pr^{3+}$ content in sample 2 was determined using atomic-emission spectroscopy. The effective distribution coefficient $k_{\mathrm{ef}}$ was found from the Gulliver–Pfann equation [13] using experimental $Pr^{3+}$ concentrations $C_{\mathrm{Pr}}$ in the crystal as a function of the relative coordinate of the boule crystallized section *g* (Fig. 2). The quantity *g* was defined as the ratio of the crystal section coordinate for which the concentration measurements were made to the whole length of the grown crystal (boule).

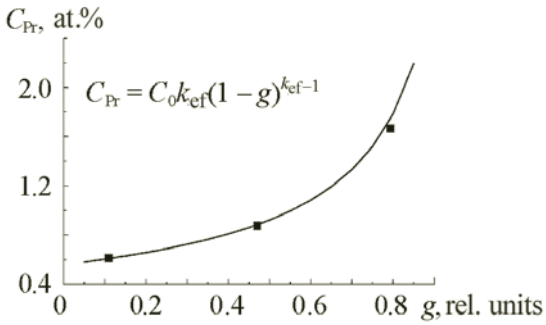


Fig. 2. $Pr^{3+}$ content in $LiY_{0.3}Lu_{0.7}F_4$ crystal as a function of relative coordinate of boule crystallized section *g*; points are experimental data.

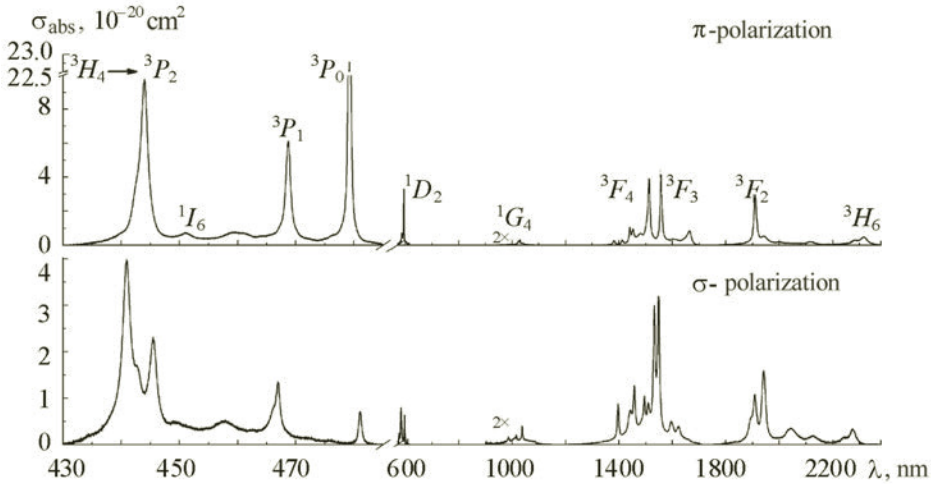


Fig. 3. $LiY_{0.3}Lu_{0.7}F_4$:$Pr^{3+}$ crystal absorption cross-section spectra.

TABLE 1. Absorption Properties of Fluoride Crystals with the Scheelite Structure and $Pr^{3+}$ Ions

| Transition | | λ, nm | | | Δλ, nm | | | $\sigma_{abs}$, · $10^{-20}$ cm$^2$ | | |
|---|---|---|---|---|---|---|---|---|---|---|
| | | YLF | LLF | $LiY_{0.3}Lu_{0.7}F_4$ | YLF | LLF | $LiY_{0.3}Lu_{0.7}F_4$ | YLF | LLF | $LiY_{0.3}Lu_{0.7}F_4$ |
| $^3H_4 \rightarrow {}^3P_2$ | σ | 441 | 440.9 | 440.9 | 1.74 | 1.94 | 1.87 | 3.9 | 4.3 | 4 |
| | π | 443.9 | 444.0 | 444.0 | 1.76 | 1.83 | 1.8 | 8.9 | 10 | 9.7 |
| $^3H_4 \rightarrow {}^3P_1$ | π | 468.7 | 468.7 | 468.7 | 0.95 | 1.0 | 1.0 | 6.3 | 6.8 | 6.1 |
| $^3H_4 \rightarrow {}^3P_0$ | π | 479.2 | 479.3 | 479.2 | 0.53 | 0.46 | 0.48 | 19.5 | 25 | 22.8 |
| $^3H_4 \rightarrow {}^1D_2$ | π | 594.6 | 594.9 | 594.8 | 1.78 | 1.8 | 1.8 | 3.0 | 3.5 | 3.3 |

The $Pr^{3+}$ distribution coefficients for YLF:Pr and LLF:Pr crystals were $k = 0.15$ and 0.22 [14]. An approximation gave $k_{ef} = 0.28$, which indicated that the $Pr^{3+}$ distribution coefficient increased in the studied crystal composition.

Figure 3 shows absorption cross sections $\sigma_{abs}$ for $LiY_{0.3}Lu_{0.7}F_4$:$Pr^{3+}$ crystal in the visible and IR regions for σ- and π-polarizations. The obtained functions were analogous to those for YLF:Pr and LLF:Pr crystals [15] although the studied crystal had intermediate absorption cross sections (Table 1). Transitions $^3H_4 \rightarrow {}^3P_0$ and $^3H_4 \rightarrow {}^3P_2$ that are used to pump Pr lasers were most interesting. The maximum absorption cross sections were $22.8 \cdot 10^{-20}$ and $9.7 \cdot 10^{-20}$ cm$^2$ for π-polarization at $\lambda = 479.2$ and 444.0 nm.

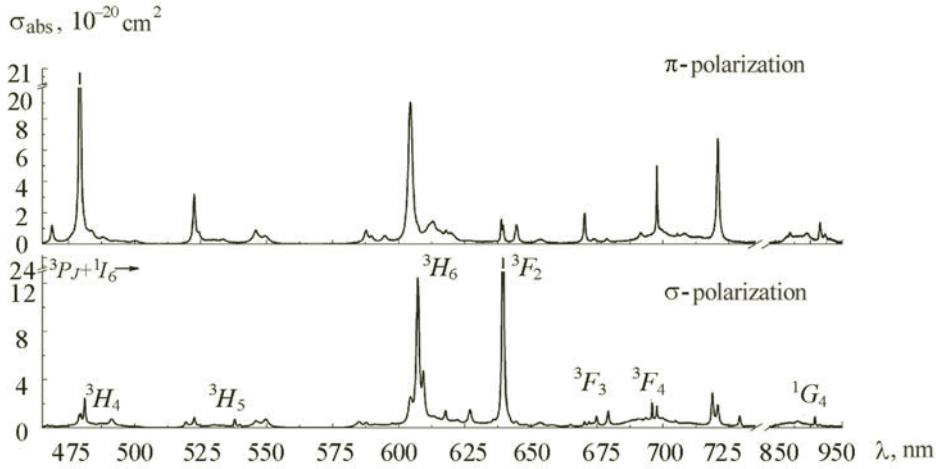


Fig. 4. $LiY_{0.3}Lu_{0.7}F_4:Pr^{3+}$ crystal stimulated emission cross-section spectra.

TABLE 2. Theoretical and Experimental Oscillator Strengths of $LiY_{0.3}Lu_{0.7}F_4:Pr^{3+}$ Crystal

| Transition $^3H_4 \rightarrow$ | $\bar{\lambda}$, nm | $f_{exp} \cdot 10^{-6}$ | $f_{ICI} \cdot 10^{-6}$ |
|---|---|---|---|
| $^3H_6$ | 2194 | 0.5 | 0.385 |
| $^3F_2$ | 1928 | 1.38 | 1.378 |
| $^3F_3 + {}^3F_4$ | 1530 | 8.09 | 8.13 |
| $^1G_4$ | 1031 | 0.146 | 0.393 |
| $^1D_2$ | 589 | 3.24 | 3.247 |
| $^3P_0 + {}^3P_1 + {}^1I_6$ | 472 | 5.23 | 5.228 |
| $^3P_2$ | 443 | 10.73 | 10.881 |

Table 2 presents oscillator strengths $f_{exp}$ determined using Eq. (2) and theoretical $f_{ICI}$. It is noteworthy that $f_{ICI}$ includes oscillator strengths of both ED and MD transitions, if present. Fitting gave $\Omega_2 = 0.082 \cdot 10^{-20}$ cm$^2$, $\Omega_4 = 2.782 \cdot 10^{-20}$cm$^2$, $\Omega_6 = 17.20 \cdot 10^{-20}$ cm$^2$, $R_2 = 0.135 \cdot 10^{-4}$ cm$^{-1}$, $R_4 = -0.039 \cdot 10^{-4}$ cm$^{-1}$, $R_6 = 0.313 \cdot 10^{-4}$ cm$^{-1}$, and mean-square deviation MSD = $0.646 \cdot 10^{-20}$ cm$^2$.

Figure 4 shows stimulated emission (SE) cross sections $\sigma_{SE}$ that were calculated using the Füchtbauer–Ladenburg equation and the corrected spectra [16]. Luminescence spectra of $Pr^{3+}$ exhibited several bands from metastable state $^3P_0$ and states $^3P_1$ and $^1I_6$ that were thermally coupled with it [17]. The maximum cross sections for each transition were comparable to those for YLF:Pr and LLF:Pr crystals [15]. Table 3 shows that cross sections did not differ substantially among crystals.

Figure 5 shows the luminescence decay kinetics from the set of $^3P_J$ upper states. The measured lifetime for sample 1 was 43 μs (single-exponential decay kinetics); for sample 2, 30 μs. However, the decay kinetics for sample 2 were not single-exponential because of cross relaxations ($^3P_0 + {}^1D_2 = {}^3H_4 + {}^3H_5$ and $^3P_0 + {}^1G_4 = {}^3H_4 + {}^1G_4$) that caused luminescence quenching [15]. The radiative lifetime obtained from *f–f*-transition intensity theory was 39 μs, which was slightly less than the analogous time for YLF:Pr and LLF:Pr crystals (~50 μs) [15].

A thermally stabilized InGaN-LD with output power up to 4 W and $\lambda_{em}$ = 444 nm was used as the pump in laser experiments. Pump radiation was focused on the active element in a square spot (~80 × 80 μm). The active element was a $LiY_{0.3}Lu_{0.7}F_4:Pr^{3+}$ crystal (10 mm, sample 1) with anti-reflection coatings on the end faces. The active element was placed into a three-mirror cavity formed by plane-wave and exit mirrors and an intracavity spherical mirror with –100 mm radius of curvature. The output mirror had 6% transmittance. The maximum output power was 0.38 W with slope efficiency 19% (Fig. 6). The absorbed pump power of 3.9 W corresponded to optical efficiency ~10%. Pump quality parameter $M^2 \leq 1.2$ so that the beam was elliptical and parallel to the crystal optical axis

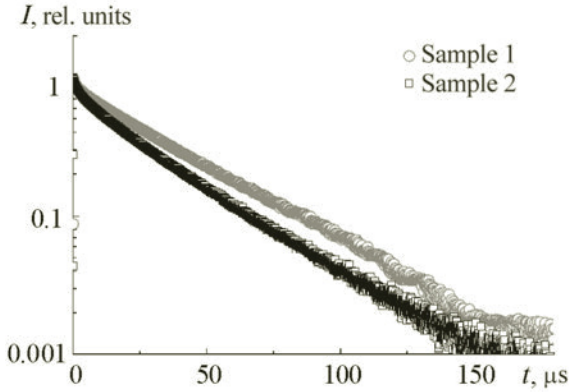


Fig. 5. Luminescence decay kinetics of the $^3P_J$ level in $LiY_{0.3}Lu_{0.7}F_4:Pr^{3+}$ crystal.

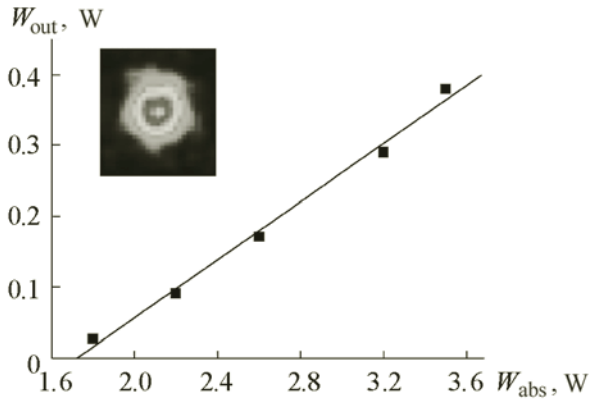


Fig. 6. Output characteristics of $LiY_{0.3}Lu_{0.7}F_4:Pr^{3+}$ crystal laser.

TABLE 3. Luminescence Characteristics of Fluorides with the Scheelite Structure and $Pr^{3+}$

| Transition | | λ, nm | | | Δλ, nm | | | $\sigma_{SE}$, $10^{-20}$ cm$^2$ | | |
|---|---|---|---|---|---|---|---|---|---|---|
| | | YLF | LLF | $LiY_{0.3}Lu_{0.7}F_4$ | YLF | LLF | $LiY_{0.3}Lu_{0.7}F_4$ | YLF | LLF | $LiY_{0.3}Lu_{0.7}F_4$ |
| $^3P_J \rightarrow H_4$ | π | 479.2 | 479.3 | 479.3 | 0.75 | 0.85 | 0.85 | 19.4 | 19.7 | 20.5 |
| | σ | 481.1 | 481.1 | 481.1 | 0.77 | 0.9 | 0.86 | – | 2.1 | 2.4 |
| $^3P_J \rightarrow {}^3H_5$ | π | 522.6<br>545.9 | 522.6<br>546.2 | 522.6<br>546 | 1.11<br>5.6 | 1.15<br>5.6 | 1.13<br>5.6 | 2.6<br>0.8 | 2.4<br>0.8 | 2.9<br>0.9 |
| $^3P_J \rightarrow {}^3H_6$ | π | 604.3 | 604.1 | 604.2 | 1.9 | 1.91 | 1.92 | 9.8 | 9.3 | 9.0 |
| | σ | 607.2 | 607.1 | 607.1 | 1.25 | 1.46 | 1.4 | 11.3 | 11.8 | 12.3 |
| $^3P_J \rightarrow {}^3F_2$ | σ | 639.5 | 640.1 | 640 | 0.78 | 0.8 | 0.8 | 21.8 | 21 | 23.6 |
| $^3P_J \rightarrow {}^3F_3$ | π | 670.3<br>697.6 | 670<br>697.8 | 670<br>697.8 | 0.75<br>0.44 | 0.98<br>0.6 | 0.55<br>0.6 | –5.2 | 1.4<br>4.3 | 1.9<br>4.9 |
| $^3P_J \rightarrow {}^3F_4$ | π | 720.8 | 721.4 | 721.2 | 0.97 | 1.1 | 1 | 8.8 | 7.2 | 6.7 |
| | σ | 718.7 | 719 | 719 | 0.86 | 0.9 | 0.88 | – | 2.8 | 2.9 |
| $^3P_J \rightarrow {}^1G_4$ | π | 915 | – | 915 | – | – | 4 | – | – | 1.4 |

It is noteworthy that the rather low efficiency was due to suboptimal locking of the pump and generation modes because of the rectilinear cross-sectional profile of the pump beam. This increased the pump beam size by 2.5 times at the edges of the active element in the meridional plane. Future work will be aimed at optimizing the pump system and cavity and active-element configurations.

**Conclusions.** $LiY_{0.3}Lu_{0.7}F_4:Pr^{3+}$ crystals were grown by the Bridgman–Stockbarger method and were characterized with a Pr effective distribution coefficient of 0.28. The absorption transitions used for pumping Pr lasers had maximum cross sections of $22.8 \cdot 10^{-20}$ cm$^2$ and $9.7 \cdot 10^{-20}$ cm$^2$ for π-polarization at λ = 479.2 and 444.0 nm. Absorption transition oscillator strengths were determined experimentally and used to find intensity parameters from *f–f*-transition intensity theory. Stimulated emission cross-section spectra were calculated using corrected luminescence spectra and the Füchtbauer–Ladenburg equation. The lifetime of an excited state $^3P_J$ depended on the $Pr^{3+}$ content and was 43 μs for a sample with distribution coefficient 0.28. Continuous generation at λ = 522.6 nm ($^3P_1 \rightarrow {}^3H_5$ transition) with maximum output power 0.38 W and slope efficiency 19% for output mirror transmittance 6% was obtained with pumping by a GaN-diode laser.

**Acknowledgment.** The work was financially supported by a grant to Kazan Federal University for a State Task for Scientific Activity (Project No. 3.1156.2017/4.6).

## REFERENCES

1. C. Krankel, D.-T. Marzahl, F. Moglia, G. Huber, and P. Metz, *Laser Photonics Rev.*, **10**, 548–564 (2016).
2. P. Metz, F. Reichert, F. Moglia, S. Muller, D.-T. Marzahl, C. Krankel, and G. Huber, *Opt. Lett.*, **39**, 3193–3196 (2014).
3. T. Gun, P. Metz, and G. Huber, *Opt. Lett.*, **36**, 1002–1005 (2011).
4. S. Luo, X. Yan, Q. Cui, B. Xu, H. Xu, and Z. Cai, *Opt. Commun.*, **380**, 357–360 (2016).
5. A. S. Nizamutdinov, V. V. Semashko, A. K. Naumov, V. N. Efimov, S. L. Korableva, and M. A. Marisov, *Pis'ma Zh. Eksp. Teor. Fiz.*, **91**, 23–26 (2010).
6. M. P. Demesh S. V. Kurilchik, N. V. Gusakova, A. S. Yasukevich, V. E. Kisel, A. S. Nizamutdinov, M. M. Marisov, R. D. Aglyamov, S. L. Korableva, A. K. Naumov, V. V. Semashko, and N. V. Kuleshov, *Laser Phys.*, **28**, 045802 (2018).
7. M. A. Marisov, E. Yu. Koryakina, A. K. Naumov, V. V. Semashko, S. L. Korableva, and N. G. Ivoilov, *Proc. SPIE Int. Soc. Opt. Eng.*, **7994**, 79940F (2010).
8. A. A. Lyapin, V. G. Gorieva, S. L. Korableva, S. A. Artemov, P. A. Ryabochkina, and V. V. Semashko, *Laser Phys. Lett.*, **13**, 125801 (2016).
9. V. V. Semashko, S. L. Korableva, A. S. Nizamutdinov, S. V. Kuznetsov, A. A. Pynenkov, P. A. Popov, A. E. Baranchikov, K. N. Nishchev, V. K. Ivanov, and P. P. Fedorov, *Russ. J. Inorg. Chem.*, **63**, No. 4, 433–438 (2018).
10. M. P. Demesh, N. V. Gusakova, A. S. Yasyukevich, N. V. Kuleshov, S. V. Grigor′ev, Yu. A. Krot, M. B. Kosmyna, and A. N. Shekhovtsov, *Prib. Metody Izmer.*, **6**, 211–219 (2015).
11. J. D. Axe, *J. Chem. Phys.*, **39**, 1154–1160 (1963).
12. A. A. Kornienko, A. A. Kaminskii, and E. B. Dunina, *Phys. Status Solidi B*, **157**, 267 (1990).
13. W. G. Pfann, *JOM*, **4**, 747–753 (1952).
14. F. Cornacchia, A. DiLieto, M. Tonelli, A. Richter, E. Heumann, and G. Huber, *Opt. Express*, **16**, 15932–15941 (2008).
15. A. Richter, *Laser Parameters and Performance of $Pr^{3+}$-Doped Fluorides Operating in the Visible Spectral Region*, Doctoral Dissertation, Hamburg, 2008.
16. S. A. Payne, L. L. Chase, L. K. Smith, W. L. Kway, and W. F. Krupke, *IEEE J. Quantum Electron.*, **28**, 2619–2630 (1992).
17. J. L. Adam, W. A. Sibley, and D. R. Gabbe, *J. Lumin.*, **33**, 391–407 (1985).